ACS OMEGA

http://pubs.acs.org/journal/acsodf

Article

Vapor Deposition-Prepared MIL-100(Cr)- and MIL-101(Cr)-Supported Iron Catalysts for Effectively Removing Organic Pollutants from Water

Huimin Zhuang,[‖] Wumin Zhang,[‖] Lu Wang, Yuanyuan Zhu, Yanyan Xi, and Xufeng Lin*

Cite This: *ACS Omega* 2021, 6, 25311−25322

Read Online

ACCESS | Metrics & More | Article Recommendations

ABSTRACT: Metal organic framework (MOF)-supported Fe catalysts belong to an important class of catalysts used for the advanced oxidation of organic pollutants in water. The successful preparation of the Fe/MIL-100(Cr) and Fe/MIL-101(Cr) catalysts in this work reinforced that a recently established carrier-gas free vapor deposition method can be a general one for preparing Fe/MOF catalysts. The Fe loading was in the range of 7.8−27.2 wt % on Fe/MIL-101(Cr) at a deposition temperature of 110−150 °C, and it was only 4.35 wt % on Fe/MIL-100(Cr) at 110 °C in comparison. The results obtained from the characterization using the N_2-isotherm and EDX mapping showed that the Fe components resided uniformly within the pore of the MOF supports. Both of Fe/MIL-100(Cr) and Fe/MIL-101(Cr) were rather effective for the catalytic removal of aniline from water with Fenton oxidation. Fe/MIL-100(Cr) can effectively remove the total organic carbon (TOC) of the aniline solutions, while Fe/MIL-101(Cr) had a lower TOC removal efficiency. Both of the Fe/MIL-100(Cr) and Fe/MIL-101(Cr) catalysts showed good stability in the crystalline form compared to the previously prepared Fe/UiO-66 catalyst, implicating that they can be potentially more useful than Fe/UiO-66 for treating organic pollutants in water.

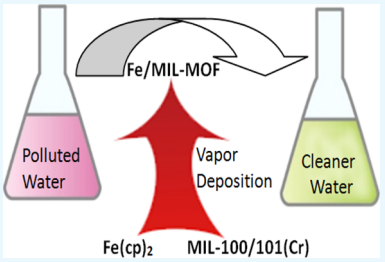

1. INTRODUCTION

Global water pollution has become a serious problem for humanity in the present days. The ever-increasing demand for clean water has triggered extensive research on the advanced technologies for water treatment.[1−3] Among the various types of water pollutants that critically require reducing, organic pollutants belong to an important and widely occurring type. Organic pollutants in general, when drained into the waters in the ground, increase the nutrition in water, and subsequently often lead to a dramatic growth of hydrophytes such as algae. Then, the hydrophytes can consume a large amount of oxygen in water, which in turn can cause the death of a large number of aquatic animals such as fishes. In particular, benzene-ring-containing compounds such as aniline and some dyes are often toxic, non-biodegradable, and even carcinogenic to human being.[4−7] Techniques for removing organic pollutants from water can be classified as physical, chemical, and biological ones. Among these three types of technology for water treatment, the advanced oxidation processes (AOPs) (e.g., Fenton and electro-Fenton processes and wet air oxidation) are of great practical importance due to their advantages such as strong oxidative capacity, wide applicability, mild reaction conditions, and being able to reduce non-biodegradable organics[8−10] Homogeneous Fe^{3+} catalysts are generally used in a conventional Fenton reaction,[11−14] where organic compounds are oxidized by H_2O_2. However, the conventional Fenton reaction often requires a rigorous pH value (always around ∼3), further treatment of Fe-containing liquid/sludge, and high operating costs especially in a large scale application.[12,15,16]

In order to efficiently remove organic pollutants in aqueous solution with the AOP methods, combination of technologies has been developed, such as the photo-assisted Fenton process,[17,18] the electrochemical-assisted Fenton process, and the sonochemical-assisted Fenton process to enhance the generation of $^{\bullet}OH$, and thus improve the utilization of H_2O_2.[19] On the other hand, great efforts have been devoted to develop heterogeneous solid catalysts to overcome the drawbacks of homogeneous catalysts. Yu et al.[17] used Fe_3O_4−GO as a heterogeneous photo-Fenton catalyst for the oxidative degradation of phenol. They showed that under optimal conditions with UV-light irradiation, about 98.8% phenol and 81.3% total organic carbon (TOC) of a phenol solution can be removed after a 120 min degradation process. Because the Fe component is effective in catalyzing the generation of $^{\bullet}OH$ from H_2O_2, various kinds of Fe-based heterogeneous catalysts have been developed for Fenton-like reactions so far, such as

Received: June 14, 2021
Accepted: September 16, 2021
Published: September 24, 2021

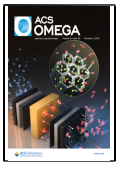

ferrocene,[20] iron oxide,[21] FeO_x/SiO_2,[22] β-FeOOH/rGO,[23] Fe/SBA-15,[24] ascorbic acid/Fe@Fe_2O_3,[25] and so forth. For example, Shukla et al.[24] found that Fe/SBA-15 can show a 100% DCP conversion and a 60% TOC removal under the conditions of 100 ppm DCP and 0.05 g 10 wt % Fe/SBA-15. However, as a whole, the catalytic performance of the presently reported heterogeneous Fe catalysts in the literature still needs further improvement in order to meet the requirements of commercial applications, which requires people to develop more types of novel heterogeneous Fe catalysts.

Metal−organic frameworks (MOFs), being highly porous crystalline materials, have attracted great interest in the field of sustainable energy and environmental problems.[26−28] MOF-based materials have been widely applied in various fields such as gas storage,[29,30] separation,[31,32] adsorptive removal of toxic species,[33−36] and heterogeneous catalysis.[1,37−46] In particular, for the heterogeneous catalytic degradation of organic pollutants and other toxic compounds in water, either in the presence or absence of light irradiation, the Fe-based MOFs (especially, MIL family MOFs) have been extensively studied in recent years. For instance, Wang et al.[37] synthesized a WO_3/MIL-100(Fe) composite with ball-milling, and this composite showed superior performance for simultaneous removal of Cr(VI) and bisphenol A under visible light irradiation. Liu et al.[41] reported that the MIL-88(Fe)/GO−H_2O_2 systems exhibited significantly higher photocatalytic activity toward degrading rhodamine B (RhB) than bare MIL-88A(Fe)−H_2O_2 under visible light irradiation. Zhao et al.[44] showed that the methylene blue removal through adsorption by MIL-100(Fe) and Fe^{II}@MIL-100(Fe) was, respectively, 27 and 6% in 30 min; however, Fe^{II}@MIL-100(Fe) exhibited highest Fenton catalytic ability compared to the MIL-100(Fe) and Fe_2O_3 catalysts. Moreover, Fe^{II}@MIL-100(Fe) retained the catalytic performance in a wide pH range of 3−8, and had a relatively low iron leaching even under acidic conditions. Ai et al.[1] demonstrated that a Fe terephthalate MOF, MIL-53(Fe), was capable of activating H_2O_2 to achieve a high efficiency in a photocatalytic process. It can completely decompose 10 mg/L RhB in the presence of a certain amount of H_2O_2 under visible light irradiation within 50 min. Vu et al.[46] reported that the partial isomorphous substitution of Cr by Fe in the MIL-101 framework was succeeded by a direct synthesis using a hydrothermal method, and an amount of ca. 25% of Cr atoms in the MIL-101 framework was substituted by Fe atoms. Fe−Cr-MIL-101 showed a high adsorption capacity of a reactive dye, RR195. Moreover, this material exhibited high photo-Fenton activity and high stability in reactive dye degradation, opening up the new application of MOFs as a novel heterogenous photo-Fenton catalyst. It is generally believed that Fe-based MOFs possess not only abundant exposed active Fe sites for a heterogeneous Fenton reaction but also have a favorable accessibility for reactants to active sites, making them promising Fenton-like catalysts for wastewater treatment. However, most of the MOF materials with low thermal and/or hydrolytic stability[47] may lead to metal-active sites being blocked by the organic linker or solvent.

There are two strategies when using MOFs as catalysts (or adsorbents) in the place of the catalytically (or adsorptively) active components.[30,33−43] The first strategy is that the MOFs' ingredients, especially their metal sites, are catalytically or adsorptively active.[30,35] The second one is that MOFs' ingredients are not necessarily active for catalysis, and instead, the active components are introduced and made to reside on the surface of MOFs. The other strategy using a MOF as one ingredient for a composite,[33,34,37−40] for example, PANI/MIL-88A(Fe) reported by Wang et al.[38] or ZIF-67@animated chitosan reported by Omer et al.,[33] actually has its roots from one of the above two strategies. Obviously, the second strategy allows people to have wider options in the selection of MOF type than the first one. For this goal, our group has developed a carrier-gas-free vapor deposition (VD) method[48] for preparing UiO-66-supported Fe catalysts (Fe/UiO-66).[49] The obtained Fe/UiO-66 catalyst presented a superior performance in catalytic oxidation of aqueous organic compounds compared to Fe-containing MOFs reported in the literature.[1,44,45,50] However, the stability of Fe/UiO-66 was found to be poor (vide infra). In addition, in these previous works, the degradation of organic pollutants catalyzed by Fe/UiO-66 was simply evaluated by measuring the chemical oxygen demand (COD) values in the aqueous solutions. The study on the mineralization efficiency of organic pollutants, which can be evaluated by the TOC values, was not shown.

In this context, it is interesting to extend the carrier-gas free VD preparation method to the MOFs other than UiO-66. Through such kinds of work, this preparation method may be reinforced to be a general method for preparing MOF-supported Fe catalysts. On the other hand, by a careful selection of the type of the MOF material, the VD-prepared Fe/MOF catalyst may show better performances for the catalytic degradation of organic pollutants in water. In this work, MIL-100(Cr)[51] and MIL-101(Cr)[52] were selected as the supporting materials, both of which had a larger specific surface area and better thermal stability than UiO-66. The prepared catalysts were characterized and their catalytic performances in organic pollutant degradation were evaluated systematically. In particular, Fe/MIL-101(Cr) exhibited excellent catalytic properties in terms of degradation of methyl orange (MO) and aniline.

2. EXPERIMENTAL SECTION

2.1. Materials and Catalyst Preparation. The chromium terephthalate-based MOF [MIL-101(Cr)] and hybrid chromium carboxylate [MIL-100(Cr)] were purchased from Beijing Huawei Ruike Chemical Co, Ltd. Ferrocene ($C_{10}H_{10}Fe$), MO ($C_{14}H_{14}N_3NaO_3S$), aqueous hydrogen peroxide solution (H_2O_2, 30 wt %), and aniline were purchased from Sinopharm Chemical Reagent Co, Ltd. All chemicals were of analytical grade and used without further treatment. The deionized (DI) water was used throughout the experiments.

Fe/MIL-101(Cr) was synthesized with a carrier-gas-free VD method that was used for the preparation of Fe/UiO-66 previously.[49] Ferrocene was also used as the Fe precursor and MIL-101(Cr) was used as the catalyst support. The whole preparation process consists of the following steps. First, a watch glass containing 1.0 g MIL-101(Cr) powder was heated at 120 °C in air for 6 h to remove the moisture. This step was named as "precalcination" hereafter because it was performed before the VD step. Second, after cooling down, the watch glass containing precalcined MIL-101(Cr) was quickly placed at the center of a Petri dish having an appropriate size, and then 2.0 g of ferrocene powder was spread evenly around the inside edge of the watch glass. Then, the Petri dish was covered firmly. The whole Petri dish setup before the VD step is depicted in Figure 1a. The third step was the VD step. In this step, the whole Petri dish setup was heated at a temperature

https://doi.org/10.1021/acsomega.1c03118
ACS Omega 2021, 6, 25311−25322

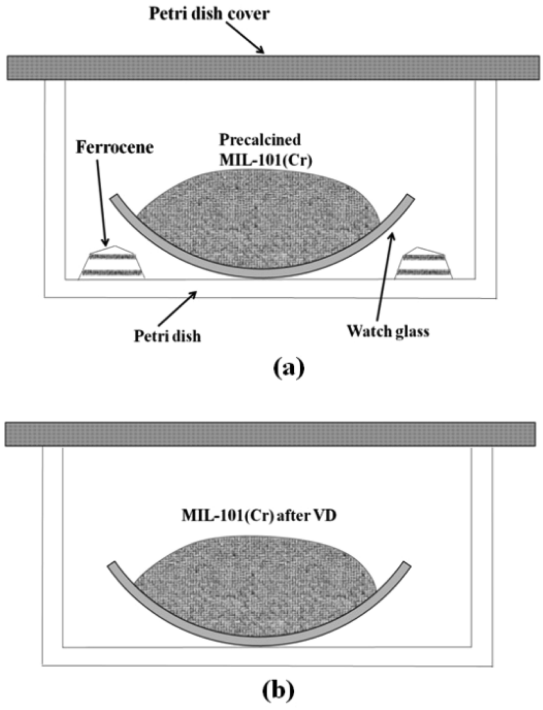

Figure 1. Simple schematic diagrams of the key steps for VD preparation of the Fe/MIL-101(Cr) catalyst, close to a procedure as reported previously in our group.[49] Panel (a) depicts the setup used immediately before and during the VD step, (b) setup for the calcination after the VD step, see the whole preparation process in detail in the text.

(denoted as T_d) of 110−150 °C for 2 h. Fourth, after cooling down, the Petri dish was uncovered, and the remaining ferrocene on the wall of glass vessels was carefully removed. Then, the Petri dish was covered again, as shown in Figure 1b, and the whole Petri dish was calcined at 180 °C for 1 h. Then, a brown color target catalyst was obtained, and it was denoted as Fe/MIL-101(Cr) in this paper. The preparation method of the Fe catalyst supported on MIL-100(Cr) [denoted as Fe/MIL-100(Cr)] was similar to that of the Fe/MIL-101(Cr) catalyst, with the only difference being that MIL-100(Cr) was replaced for MIL-101(Cr).

2.2. Catalyst Characterization. The crystal structure of the prepared samples was evaluated by powder X-ray diffraction (XRD, D8 Advance, Germany) using Cu Kα radiation (λ = 0.15418 nm) at 40 kV, 30 mA, with a scan step of 0.02° and 2θ ranging from 5 to 75°. The morphology and structure of the prepared catalysts were measured using a field-emission scanning electron microscope (Hitachi SU3500). The 77 K-N_2 adsorption−desorption isotherm of a certain sample was measured by using an ASAP2010 instrument. Then, the specific surface area and pore-size distribution of these catalysts were calculated using the Brunauer−Emmett−Teller (BET) method for the adsorption branch and the Barrett−Joyner−Halenda (BJH) method for the desorption branch, respectively.

The MOF-supported Fe catalyst was treated to form an aqueous solution before its Fe content was measured. In a typical treatment process, ∼2 mg catalyst was placed in a polytetrafluoroethylene (PTFE) beaker containing a small amount of DI water. Then, concentrated nitric acid (∼67%, 4 mL), concentrated hydrofluoric acid (∼40%, 4 mL), and concentrated perchloric acid (∼71%, 0.5 mL) were added to the PTFE beaker. This beaker was then heated, and during this heating process the solid sample became dissolved accompanied by white smoke. After the white smoke was exhausted, two drops of hydrochloric acid (∼18 wt %) was added to dissolve the solid residue. The beaker was kept heated until a clear liquid solution was obtained and no solid can be observed. This liquid solution was transferred to a volumetric flask, and diluted to 100.0 mL with DI water. In this flask, ascorbic acid was added to keep the Fe species in the status of Fe(II) in the solution, and phenanthroline was added as the chromogenic agent of the Fe species (the characteristic absorption band is located at 510 nm). The Fe concentration of the diluted solution, namely [Fe], was measured with atomic absorption spectroscopy by using a contrAA 700 spectrograph. A series of standard Fe solutions with known [Fe] values ranging from 0 to 100 μg Fe/g were prepared. The absorption at 510 nm of the Fe-containing solution prepared from a certain Fe/MOF sample was compared to that of the standard Fe solutions to calculate its [Fe] value. Then, the Fe content of the initial Fe/MOF catalyst, in the form of Fe wt %, can be calculated from this [Fe].

2.3. Catalytic Performance Evaluation for Organic Pollutant Degradation in Water. The catalytic performance of the Fe/MIL-101(Cr) and Fe/MIL-100(Cr) catalysts for the advanced oxidation of aqueous organic pollutants was evaluated by using a ∼250 mL flask as the reactor. In a typical catalytic experiment, a 200 mL aqueous solution of a selected organic compound was added to the reactor. The performance of the as-prepared catalyst was evaluated by degrading model polluted aqueous solution containing aniline (500 mg/L) or MO (500 mg/L). The temperature (typically being 50 °C, monitored using a temperature meter) of the reactor was controlled using a water bath. When the reaction system maintained the temperature of interest, a 2.0 mL H_2O_2 solution (30.0 wt %) was added to the above organic solution (the mixed solution had a H_2O_2 concentration of 0.087 mol/L). Upon examination, no reaction could be observed between H_2O_2 with MO or with aniline without catalyst at the reaction temperature of interest. 200 mg Fe/MIL-101(Cr) or Fe/MIL-100(Cr) was added to the reactor to initiate the catalytic oxidation reaction, and thus the dosage of the catalyst is 1000 mg/L.

After a certain reaction time, 2.0 mL liquid sample was withdrawn from the reaction mixture, and was centrifuged to remove the trace amount of solid residue. Then, this liquid sample was analyzed using a COD analyzer (HACH DR1010). The mineralization of the organic solution was evaluated on the basis of the TOC content, which was determined using a TOC analyzer (TOC-L CPH/CPN).

3. RESULTS AND DISCUSSION

3.1. Fe Content of the Catalysts. The first case of preparing an MOF-supported Fe catalyst with a carrier-gas free VD method was reported by our group previously.[49] With the motivation of extending this method to prepare more types of MOF supports and to make a general method for preparing an MOF-supported Fe catalyst, the applicability of using MIL-100 and MIL-101 in this method was examined in this work. Table 1 shows that the Fe loading of Fe/MIL-101(Cr) was between 7.8 and 27.2 wt % at a T_d of 110−150 °C. An increase in the Fe content with an increase in T_d had the same trend as the case of Fe/UiO-66; however, Fe/Fe/MIL-101(Cr) had a much

https://doi.org/10.1021/acsomega.1c03118
ACS Omega 2021, 6, 25311−25322

Table 1. Dependence of the Fe Loading of the Fe/MIL-101(Cr) Catalyst on the Deposition Temperature (T_d)

T_d (°C)	110	130	150
Fe loading (wt %)	7.8	11.6	27.2

higher Fe content at the same T_d. Interestingly, in comparison, in Fe/MIL-100(Cr) prepared by the same method, the Fe loading was only 4.4% at 110 °C. Given that most of the MOF materials have a very large surface area,[26−29,53] and the Fe loading was mainly determined by the amount of ferrocene physically adsorbed on the surface,[48] the difference in the Fe loadings on different Fe/MOF catalysts can be accounted for the specific surface area and pore volume of the MOF supports (vide infra).

3.2. Physiochemical Properties of the MOF Supports and the Fe/MOF Catalysts. The XRD patterns of the MOFs before and after VD of the Fe component are shown in Figure 2. The main characteristic peaks of the precalcined MIL-101(Cr) carrier (a precalcination temperature of 120 °C) match well with the one reported in the literature, for example, ref 54, and the peaks at 3.2, 5.0, 8.3, and 8.9° can be clearly identified in Figure 2a. All peaks of Fe/MIL-101(Cr) (T_d = 110 °C) matched well with that of the precalcinated MIL-101(Cr) carrier (precalcination temperature of 120 °C), which indicated that the entire VD process nearly did not change the crystal structure of MIL-101(Cr). No new feature in the XRD patterns associating with the resided Fe components can be observed in spite of the significant Fe loading (Table 1), indicating that the Fe components may be uniformly dispersed on the MOF surface. A similar phenomenon was observed for the case of Fe/MIL-100(Cr) preparation (Figure 2b), and thus a similar conclusion may also be plausible for the MIL-100(Cr) case. However, at a higher T_d, the crystal structure of MIL-101(Cr) tended to collapse (Figure 2a). For instance, the main peak intensity of the XRD feature of Fe/MIL-101(Cr) at a T_d of 130 °C decreased dramatically, and was almost invisible at a T_d of 150 °C. Note that when T_d = 150 °C, the Fe loading was quite high (27.2%), and it is expected that a large portion of the Fe component may reside on the outer surface of MOF. This hypothesis was supported by a significantly decreased surface area (only 89 m^2/g) for (vide infra). Hereinafter, only the results of Fe/MIL-101(Cr) and Fe/MIL-100(Cr) having a T_d of 110 °C will be shown. The adjacent peaks were clearly divided and no impurity peaks were detected, indicating the samples had good crystallization. Given that the Fe loading was rather high (7.8 wt % at T_d = 110 °C, see Table 1), the absence of a characteristic peak of Fe oxide in the XRD pattern of Fe/MIL-101(Cr) suggests that the Fe components could be rather uniformly dispersed on the MIL-101(Cr) surface (mainly the inner surface).

To support the hypothesis that the Fe component resides onto MIL-101(Cr), in particular into the inner pores, the pure MIL-101(Cr) and Fe/MIL-101(Cr) samples were analyzed using the methods of SEM, EDX, and transmission electron microscopy (TEM). Figure 3 shows the SEM images of MIL-101(Cr) and Fe/MIL-101(Cr). Figure 3a,b shows no obvious difference between the MIL-101(Cr) sample and Fe/MIL-101(Cr), indicating that the Fe-component introduction process did not noticeably alter the structure and morphology of MIL-101(Cr) in the whole VD process, partly owing to the stability of MIL-101(Cr) at the experimental temperatures. Meanwhile, the images of the MIL-100(Cr) and Fe/MIL-100(Cr) catalysts (Figure 3c,d) also did not exhibit a significant difference in the morphology. The EDX elemental mapping (Figure 4a,b) results showed that the Fe distribution of Fe/MIL-101(Cr) was well consistent with the Cr distribution in the same region. The Cr distribution was

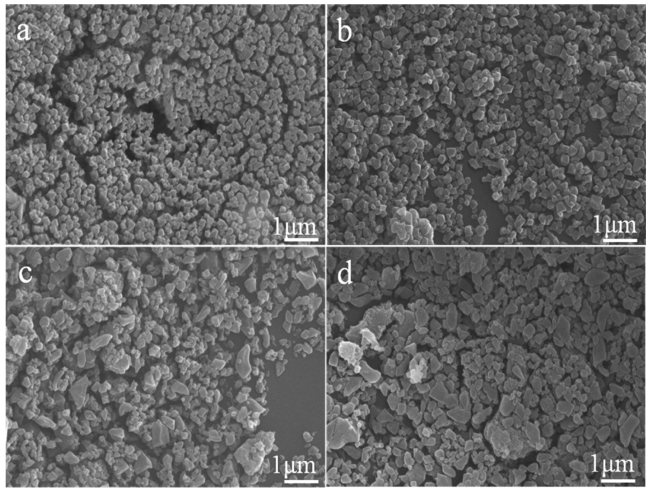

Figure 3. SEM images of (a) MIL-101(Cr) after precalcination in air at 120 °C for 6 h, (b) Fe/MIL-101(Cr) catalyst, (c) MIL-100(Cr) after precalcination in air at 120 °C for 6 h, and (d) Fe/MIL-100(Cr) catalyst.

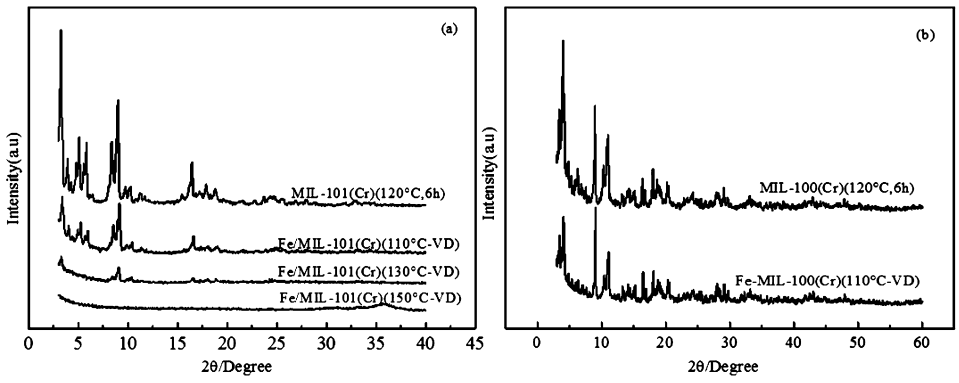

Figure 2. XRD patterns of (a) Fe/MIL-101(Cr) catalysts after VD at different deposition temperatures as indicated, compared to those of the MIL-101(Cr) sample before VD, and (b) XRD patterns of Fe/MIL-100(Cr) catalysts compared to those of the MIL-100(Cr) sample before VD.

https://doi.org/10.1021/acsomega.1c03118
ACS Omega 2021, 6, 25311−25322

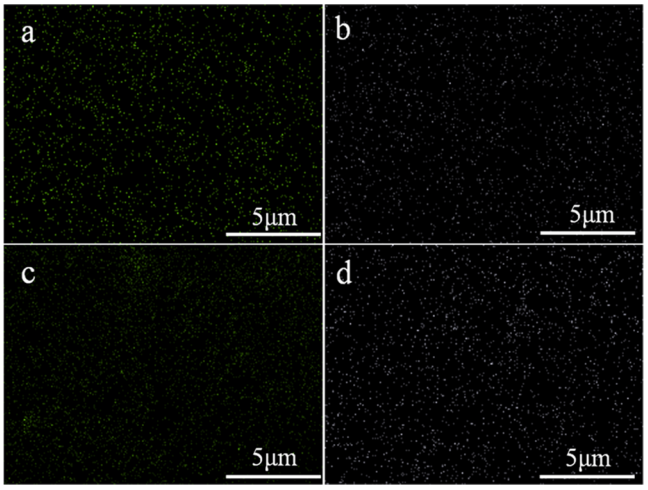

Figure 4. EDX maps of Fe/MIL-101(Cr) for (a) Cr element and (b) Fe element and of Fe/MIL-100(Cr) for (c) Cr element and (d) Fe element.

determined by the MIL-101(Cr) framework, and the EDX mapping results further indicated the uniform dispersion of the Fe element on the MIL-101(Cr) surface. It can be seen from Figure 4c,d that the Fe distribution of Fe/MIL-100(Cr) was also very consistent with the Cr distribution in the same region, which indicates the uniform dispersion of the Fe element on the MIL-100(Cr) surface. The TEM images shown in Figure 5 further confirmed this phenomenon, in which both

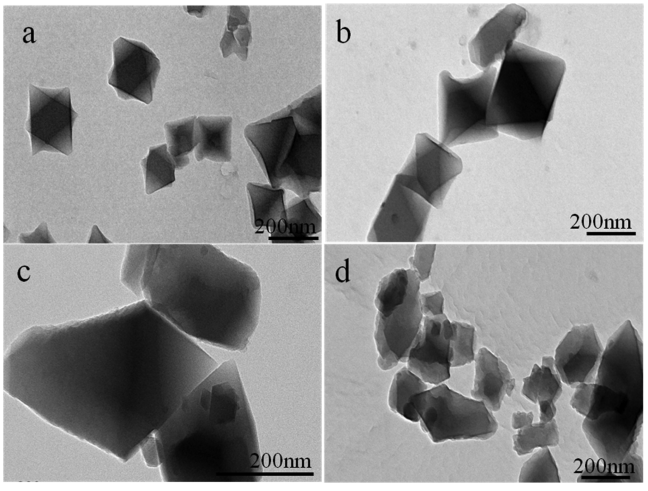

Figure 5. TEM images of (a) MIL-101(Cr) after precalcination in air at 120 °C for 6 h, (b) Fe/MIL-101(Cr) catalyst, (c) MIL-100(Cr) after precalcination in air at 120 °C for 6 h, and (d) Fe/MIL-100(Cr) catalyst.

MIL-101(Cr)[52] and Fe/MIL-101(Cr) had a good octahedral structure, while the MIL-100(Cr)[51] and Fe/MIL-100(Cr) exhibited a tetrahedral structure.

Figure 6 shows the N_2 adsorption−desorption isotherms and pore size distributions of MIL-101(Cr), Fe/MIL-101(Cr), MIL-100(Cr), and Fe/MIL-100(Cr). As shown in Figure 6a, the isotherms of MIL-101(Cr) and Fe/MIL-101(Cr) displayed a mode of type I, indicating that the materials mainly had microporous windows and possibly had a small portion of mesoporous cages.[55] At the same time, as shown in Figure 6b, the isotherms of MIL-100(Cr) and Fe/MIL-100(Cr) displayed an intermediate mode between type I and type IV, which indicated that both microporous windows and mesoporous cages did exist in the materials.[56,57] As derived from the N_2 adsorption data (Table 2), the MIL-101(Cr) material possessed a high BET surface area of 2439 m^2/g with a pore volume of 1.69 cm^3/g, while the BET surface area of the Fe/MIL-101(Cr) catalyst significantly decreased compared to the MIL-101(Cr) case. This significant decrease reflected that the Fe components introduced by VD mainly resided within the pore of MIL-101(Cr) instead of sticking to the outer surface, and the Fe loading was moderately high (7.8 wt %). This hypothesis was supported by the similarity of XRD patterns of MIL-101(Cr) and Fe/MIL-101(Cr) (Figure 2a), and also by their SEM images (Figure 3a,b). Meanwhile, it could be seen from Table 2 that the specific surface area and pore volume of the Fe/MIL-101(Cr) catalyst decreased significantly with the increase of deposition temperature (from 110 to 150 °C).

The micropore size of MIL-101(Cr) was calculated to be ~0.62 nm from the Horvath−Kawazoe analysis (Figure 6e), while the micropore size of Fe/MIL-101(Cr) was about 0.73 nm. The BJH mesopore size distribution curve exhibited a pore size centered at about 2.24 nm (Figure 6b), which was slightly larger than the MIL-101(Cr) with its maximum pore diameter of 2.11 nm. The maximum pore diameter of both MIL-101(Cr) and Fe/MIL-101(Cr) (Figure 6c) was larger than the kinetic diameter of the MO molecule (~1.4 nm).[58] The favorable structure characteristics could facilitate the contact with reactants in catalysis.

3.3. Catalytic Removal of Aniline from Water. Aniline is an important intermediate in chemical industry, especially in the field of production of polyurethanes, rubber additives, dyes, pharmaceuticals and pesticides,[59,60] as well as in the textile industry.[6] However, aniline is recognized as a major environmental pollutant because it is biorefractory and hazardous to the human health. Aniline has been frequently detected in the environment in the recent decades due to the improper discharge from industries.[61] Therefore, the removal of aniline is an important topic in the field of environmental protection,[62,63] and it is of great interest to develop novel efficient approaches to degrade aniline in wastewater.

Figure 7 shows that the COD and TOC removal rates of aniline by Fe/MIL-100(Cr) were both rather efficient at the presence of H_2O_2. The COD removal rates for both catalysts were comparable to the Fe/ZSM-5 catalyst reported by Zhu et al.[63] Parameters of the catalytic test in this work and in those of ref 63 showed that the aniline concentration in the former case (500 mg/L) was 2.5 time larger than that in the latter case (200 mg/L), and the dosage of catalyst in the former was only 1/6 of that of the latter. Furthermore, Zhu et al. explored the initial concentration of aniline, the results demonstrated that a heterogeneous Fenton-like system performed well in aniline wastewater, ranging from 100 to 400 mg/L (COD). With an increase in initial concentration, the extent of removal went down. The quantity of effective active matter, $^{\bullet}OH$, was limited to the dosage of H_2O_2, which restraining the capacity of degrading aniline.[63]

To further investigate the efficiency of the combination of H_2O_2 with Fe/MIL-100(Cr) in mineralization of aniline, TOC of the reaction was monitored and the results were illustrated in Figure 7. Although the COD and TOC removal of Fe/ZSM-5 within 120 min was larger (92.5, 72.5% respectively)[63] than that of Fe/MIL-100(Cr) (57.5, 64.5% respectively), the overall catalytic performances of these two catalysts were quite

https://doi.org/10.1021/acsomega.1c03118
ACS Omega 2021, 6, 25311−25322

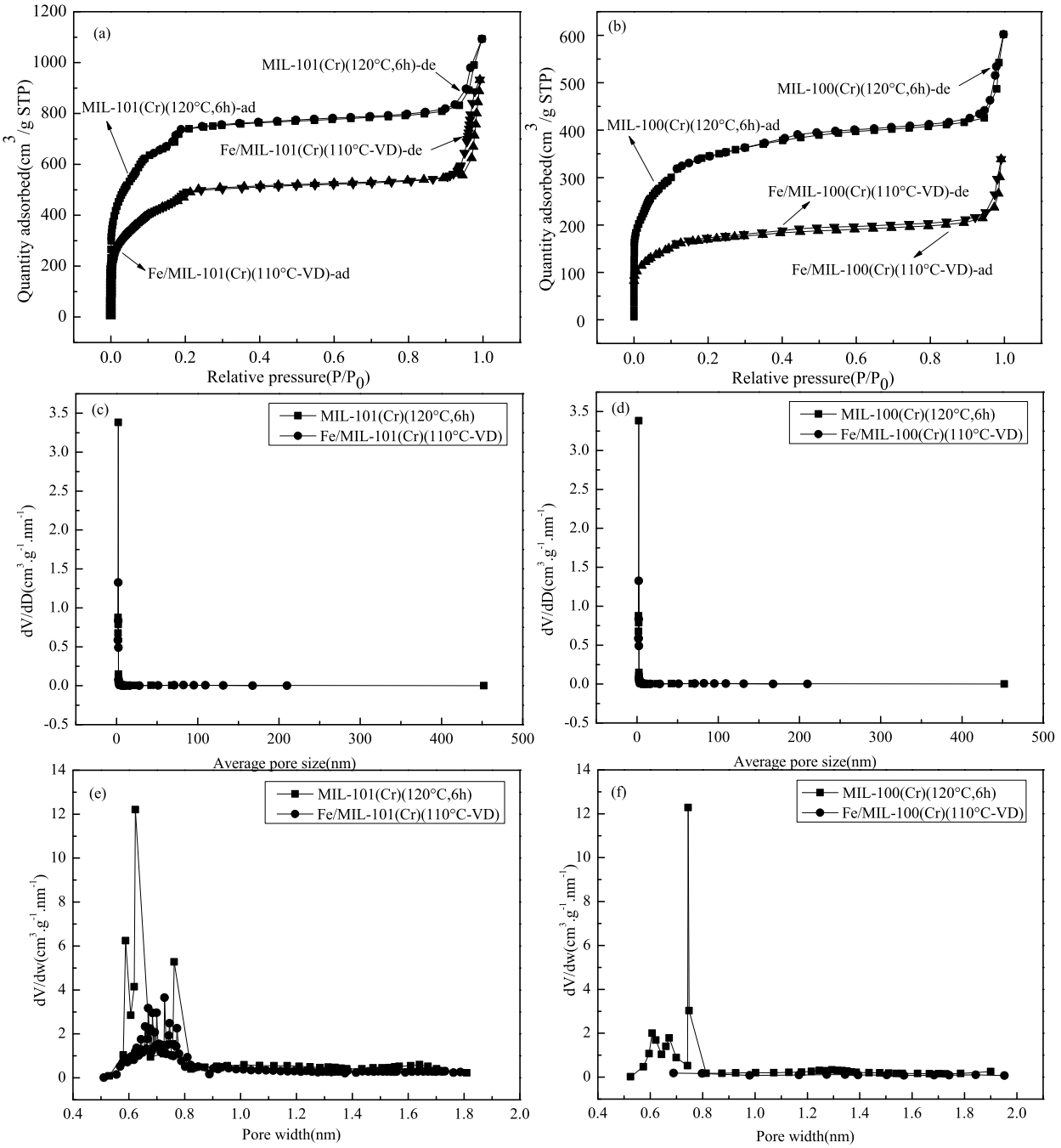

Figure 6. 77 K-N_2 adsorption−desorption isotherms of MIL-101(Cr) and Fe/MIL-101(Cr) (a), MIL-100(Cr) and Fe/MIL-100(Cr) (b); the BJH mesoporous size distribution of MIL-101(Cr) and Fe/MIL-101(Cr) (c), MIL-100(Cr) and Fe/MIL-100(Cr) (d); the HK micropore size distribution of MIL-101(Cr) and Fe/MIL-101(Cr) (e) derived from (a), and MIL-100(Cr) and Fe/MIL-100(Cr) (f) derived from (b).

comparable. Moreover, the catalytic system of aniline in this work did not require pH adjustment, while the condition of pH = 4 could be seen from the Fe/ZSM-5 catalytic system (see key information in Table 3).[63]

From the comparison between the COD and TOC removal rates for the case of Fe/MIL-100(Cr) in Figure 7, it can be demonstrated that the skeleton of aniline was destroyed and further mineralized in the Fenton-like reaction system. After 180 min of the reaction, the removal efficiency of TOC was 69.0%, which indicated that almost all aniline was mineralized into CO_2 and H_2O during the reactions.[63] In addition, the results of the reaction test, where no H_2O_2 was added, showed nearly all the COD and TOC removal rates were due to aniline being catalytically degraded instead of adsorbed by Fe/MIL-100(Cr).

The performance of the Fe/MIL-101(Cr) catalyst was also studied. It could be seen from Figure 7, within 180 min, the percentage of COD removal became higher than that of TOC, which indicates that only 29% of aniline was mineralized to CO_2, and the remaining aniline might be converted into other organics.

In order to better understand why Fe/MIL-100(Cr) can show a higher TOC removal than Fe/MIL-101(Cr) although the former presented a lower COD removal rate, a possible

https://doi.org/10.1021/acsomega.1c03118
ACS Omega 2021, 6, 25311−25322

Table 2. BET Results of the Precalcined MIL-101(Cr)(120 °C, 6 h), Fe/MIL-101(Cr)(110 °C-VD), Fe/MIL-101(Cr)(130 °C-VD), Fe/MIL-101(Cr)(150 °C-VD), MIL-100(Cr)(120 °C, 6 h), and Fe/MIL-100(Cr)(110 °C-VD) Catalysts

samples	BET surface area S_{BET} (m^2/g)	total pore volume (cm^3/g)	average pore diameter (nm)
MIL-101(Cr)(120 °C, 6 h)	2435	1.69	2.08
Fe/MIL-101(Cr)(110 °C-VD)	1683	1.44	2.20
Fe/MIL-101(Cr)(130 °C-VD)	322	0.39	2.00
Fe/MIL-101(Cr)(150 °C-VD)	98	0.36	2.34
MIL-100(Cr)(120 °C, 6 h)	1156	0.93	2.14
Fe/MIL-100(Cr)(110 °C-VD)	555	0.45	2.07

mechanistic analysis of the reaction is given below based on the mechanistic scheme shown in Scheme 1. For a given amount of H_2O_2 and aniline, three possible competing reaction pathways may occur. First, H_2O_2 may oxidize aniline to form a partially oxidized intermediate, which remained dissolved in water (with rate constant, k_1), and in this case the COD value should be decreased while the TOC value remained unchanged. Second, H_2O_2 may oxidize aniline to form the mineralized products, CO/CO_2 (with rate constant, k_2), and in this case the COD and TOC values should be decreased at the same time. The third case is that H_2O_2 underwent pure decomposition (with rate constant, k_3), and the COD and TOC values were both unchanged. The catalytic test results shown in Figure 7 reflected that Fe/MIL-100(Cr) may show a larger k_2 value than Fe/MIL-101(Cr), presenting a larger TOC removal efficiency. However, due to the second pathway consumed more H_2O_2 than the first one, the H_2O_2 concentration decreased more quickly in the Fe/MIL-100(Cr) case than in the Fe/MIL-101(Cr) case. When H_2O_2 was close to be depleted, the reaction rate would decrease sharply. This is supported by the case that when comparing the results between 2 and 3 h reactions, the Fe/MIL-100(Cr) catalyst gave a much smaller difference compared to the Fe/MIL-101(Cr) case.

3.4. Catalytic Removal of MO from Water: Catalytic Oxidation versus Adsorption. Dyes such as MO, methyl blue, and Congo red are widely used in the textile industry, and they are often difficult to be degraded biologically. To test the potential of our Fe/MOF catalyst for application in the Fenton oxidation of these dyes, the degradation of MO was performed to examine the catalytic performance of Fe/MIL-100(Cr) in a heterogeneous Fenton process. Figure 8a shows the COD removal profile of MO (500 mg/L) in the presence of H_2O_2 or without H_2O_2 using Fe/MIL-100(Cr) as a catalyst. The COD removal efficiency of MO by Fe/MIL-100(Cr), without H_2O_2, was about 28.9% within 180 min due to the adsorption of Fe/MIL-100(Cr). In comparison, when Fe/MIL-100(Cr) and H_2O_2 were added simultaneously, about 55.4% MO degradation was achieved within 180 min. This comparison showed that the contribution of the adsorption process can be rather significant to the overall COD removal of the MO solution, and Fe/MIL-100(Cr) was effective in the degradation of MO through a combination of adsorption and Fenton-like reaction. The COD removal rate of MO by Fe/MIL-100(Cr) was comparable to that by the MIL-100(Fe)/GO catalyst reported by Wang et al. (see the key information in Table 3).[64] Inspection of the catalytic test parameters in this work and those in ref 64 showed that the MO concentration in the former case (500 mg/L) was 10 time larger than that in the latter case (50 mg/L), and the dosage of H_2O_2 in both the case was equivalent. Although the degradation rate of MO within 180 min was larger (86.0%) for MIL-100(Fe)/GO than that for Fe/MIL-100(Cr) (55.4%), the overall catalytic performances of these two catalysts were quite comparable. As reported in the literature, the major degradation pathway of MO in the Fenton-like reaction is the oxidative cleavage of azo groups of MO molecules (i.e., azo double bond, −N═N−).[65,66] Furthermore, MO demonstrates two absorption bands at 467 and 273 nm. The peak at 467 nm is attributed to the azo (−N═N−) chromophore, whereas the other peak at

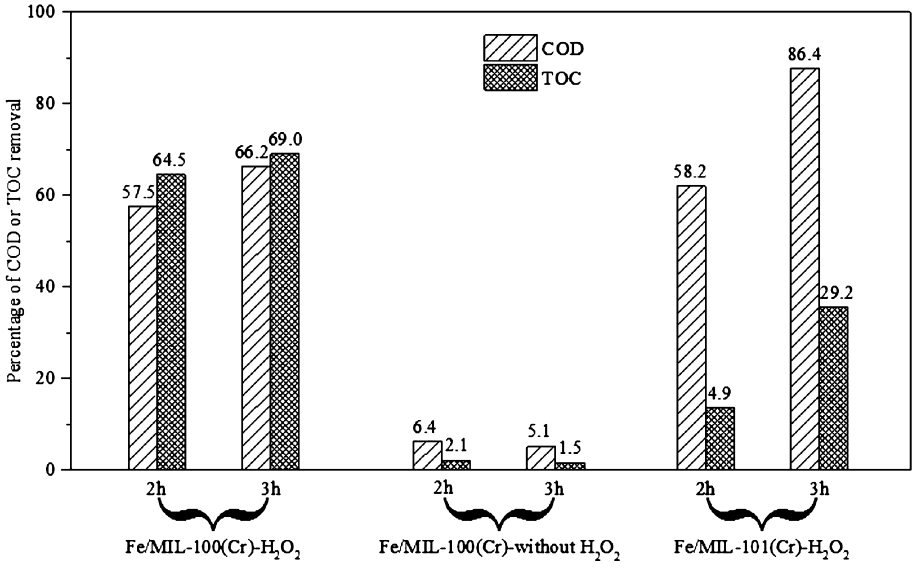

Figure 7. Catalytic removal of the COD and TOC values of aniline polluted water at the presence of H_2O_2 using Fe/MIL-100(Cr) and Fe/MIL-101(Cr) as catalysts, respectively as indicated. For comparison, the reaction test without H_2O_2 was also tested for the case of Fe/MIL-100(Cr). Reaction test conditions: aniline concentration = 500 mg/L, H_2O_2 concentration = 0.0087 mol/L, dosage of catalyst = 1000 mg/L, reaction temperature = 50 °C.

https://doi.org/10.1021/acsomega.1c03118
ACS Omega 2021, 6, 25311−25322

Table 3. Comparison of the Catalytic Test Results with a Representative Report in the Literature for Both of the Aniline and MO Systems

catalyst	COD and TOC removal %	key conditions	references
Fe/MIL-100(Cr)	57.5%, 64.5%	aniline 500 mg/L, H_2O_2 0.0087 mol/L, catalyst 1000 mg/L, 50 °C, 120 min	this study
Fe/MIL-101(Cr)	58.2%, 4.9%	aniline 500 mg/L, H_2O_2 0.0087 mol/L, catalyst 1000 mg/L, 50 °C, 120 min	this study
Fe/ZSM-5	92.5%, 72.5%	aniline 200 mg/L, H_2O_2 0.31 mL/L, catalyst 6000 mg/L, pH = 4, 120 min	63
Fe/MIL-100(Cr)	55.4%, 21.4%	MO 500 mg/L, H_2O_2 0.0087 mol/L, catalyst 1000 mg/L, 50 °C, 180 min	this study
Fe/MIL-101(Cr)	87.1%, 12.7%	MO 500 mg/L, H_2O_2 0.0087 mol/L, catalyst 1000 mg/L, 50 °C, 180 min	this study
MIL-100(Fe)/GO	86.0% (COD)	MO 50 mg/L, H_2O_2 0.0087 mol/L, catalysts 0.5 g/L, pH = 3, 180 min	64

Scheme 1. Simple Schematic Diagram for Illustrating the Possible Mechanism for Aniline Reaction with H_2O_2 in the Presence of the Fe/MIL-101(Cr) and Fe/MIL-100(Cr) Catalysts[a]

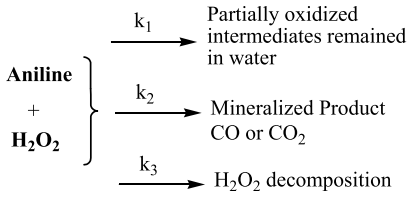

[a]Here, *k* represents the reaction rate constant for each possible route.

273 nm is associated with the aromatic ring.[3] This explains why we have previously reported that the removal rate of MO (40 mg/L) by Fe/UiO-66 within 60 min is 93% (measured using a UV−vis spectrophotometer),[49] while in this work, the COD removal rate of Fe/MIL-100(Cr) degrading high concentration MO (500 mg/L) in 180 min is 55.4% (measured using a COD meter). In other words, in the experiment of MO degradation by Fe/UiO-66, the absorbance of MO at 467 nm was measured using a spectrophotometer, and then the degradation rate was obtained according to the standard curve, that is, the degradation rate reflected the breaking of the azo group in MO. In the reaction of MO degradation by Fe/MIL-100(Cr), the COD in the MO solution was measured using a COD analyzer at a certain time. The latter can better reflect the degradation degree of organic matter (MO).

As can be seen in Figure 8a with the TOC data, it was demonstrated that in the Fenton-like system, the azo groups in MO were destroyed and further mineralized. In our work, within 180 min of the reaction, the removal efficiency of TOC was 21.7%, while the TOC removal rate in ref 49 was about 38% within 240 min. Moreover, the catalytic system for MO removal in this work did not require pH adjustment, while the condition of pH = 3 can be seen for the MIL-100(Fe)/GO catalytic system.[64]

The performance of the Fe/MIL-101(Cr) catalyst for the MO removal was also examined. It can be seen from Figure 8b that, within 180 min, the COD removal rate (87.1%) was higher than that of Fe/MIL-100(Cr) (55.4%), while the TOC removal efficiency (12.66%) was relatively much lower than that of the Fe/MIL-100(Cr) (21.7%), which indicates that only about 12.7% of MO by Fe/MIL-101(Cr) was mineralized to CO_2. However, most of the MO molecules underwent only oxidative cleavage of azo groups[65,66] or further converted into other organics.

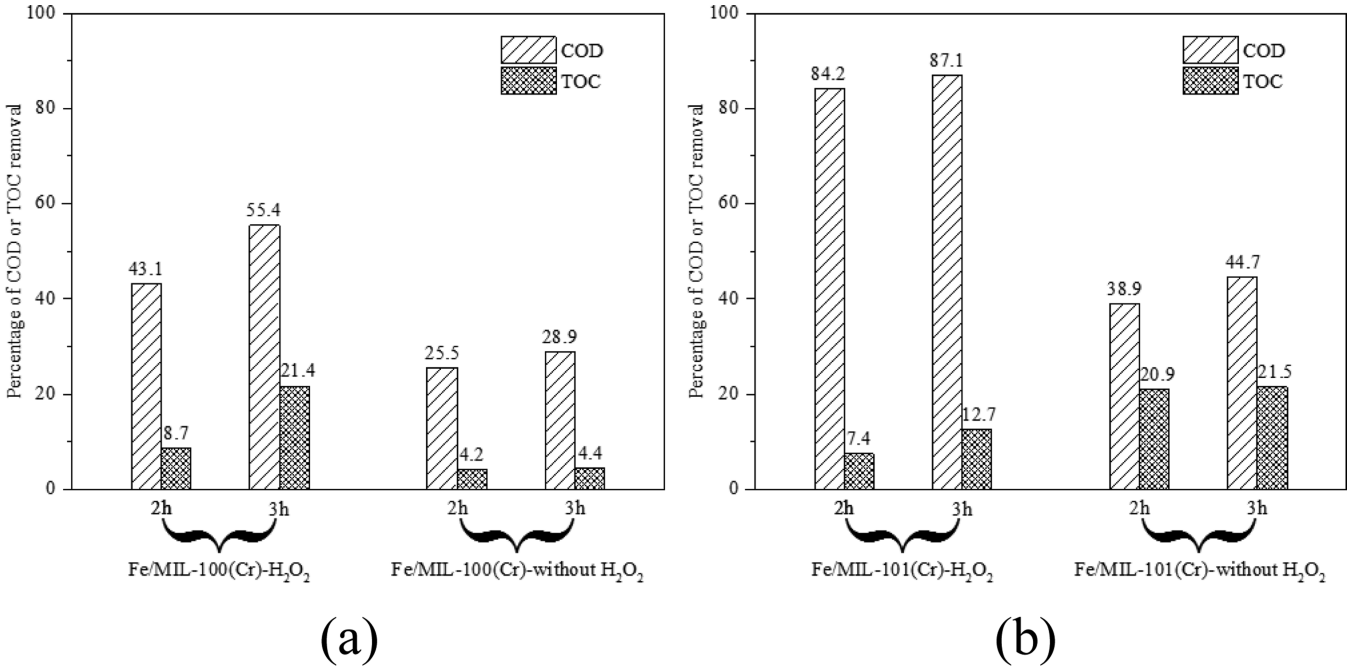

Figure 8. COD and TOC values for the catalytic removal of MO-polluted water in the presence and absence of H_2O_2 using Fe/MIL-100(Cr) (a) and Fe/MIL-101(Cr) (b) as catalysts, respectively, as indicated. Reaction test conditions: MO concentration = 500 mg/L, H_2O_2 concentration = 0.0087 mol/L, dosage of catalyst = 1000 mg/L, and reaction temperature = 50 °C.

https://doi.org/10.1021/acsomega.1c03118
ACS Omega 2021, 6, 25311−25322

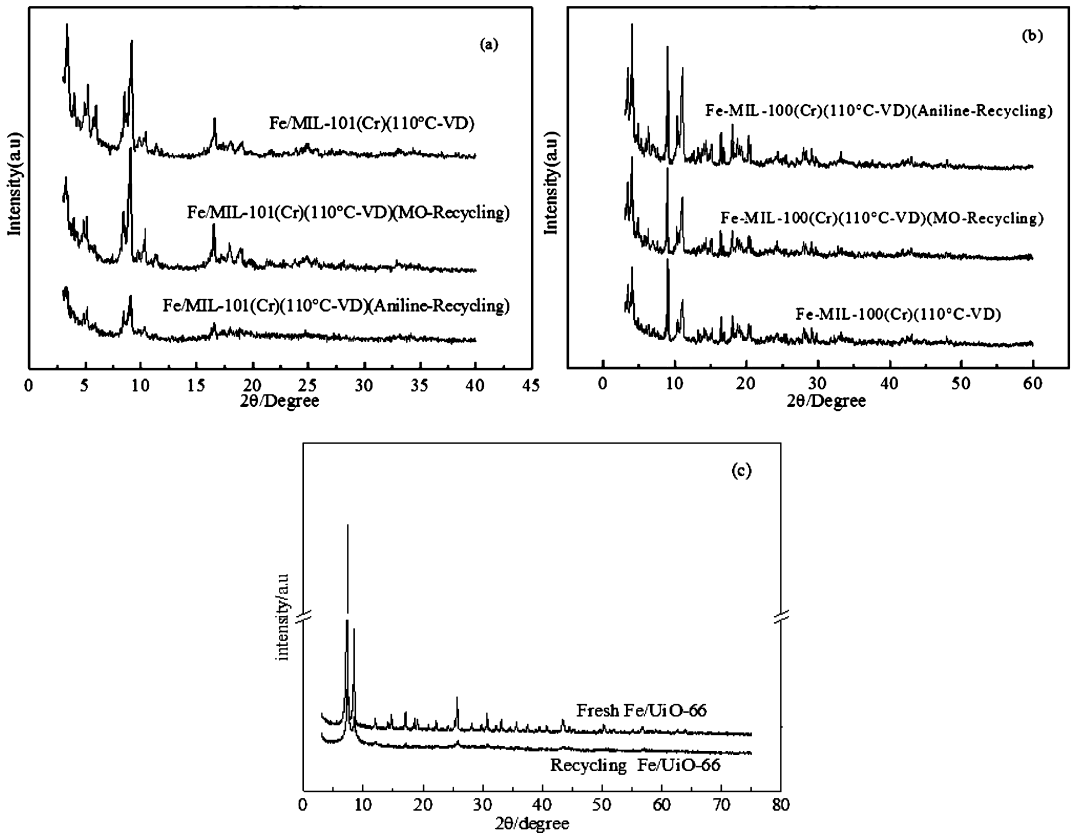

Figure 9. XRD patterns of Fe/MIL-101(Cr) (a), Fe/MIL-100(Cr) (b), and Fe/UiO-66 (c) catalysts before and after MO removal. The Fe/UiO-66 catalyst was prepared using the method reported in ref 49.

3.5. Stability of the Fe/MOF Catalysts after a Catalytic Test. Fe/MIL-101(Cr) and Fe/MIL-100(Cr) almost retained their original brown color after recycling from the catalytic evaluation system. Furthermore, the XRD patterns of the used Fe/MIL-101(Cr) and Fe/MIL-100(Cr) catalysts (after degrading of MO or aniline) were found to be similar to those of fresh samples before the reaction (see Figure 9a,b), especially the latter. The similarity indicated that there was only a slight or no obvious change in the crystal structure of these catalysts after a catalytic use in water. These results demonstrated that the Fe/MIL-100(Cr) and Fe/MIL-101(Cr) catalysts were stable under the experimental reaction conditions employed here. In comparison, recycled Fe/UiO-66 lost most of its crystal features after its use in water (see Figure 9c).

It can also be seen from Table 4 that the specific surface area and pore volume of Fe/MIL-101(Cr) recovered after degrading aniline and MO were significantly reduced compared with those of the fresh Fe/MIL-101(Cr) catalyst, which may be attributed to the adsorption of aniline and MO (including its degradation products) by Fe/MIL-101(Cr). Similarly, Fe/MIL-100(Cr) recovered after degrading aniline and MO had no significant decrease in the specific surface area and pore volume compared with the fresh Fe/MIL-100(Cr) catalyst, which further proved the excellent stability of Fe/MIL-100(Cr).

Table 4. BET Results of Fe/MIL-101(Cr) and Fe/MIL-100(Cr)(110 °C-VD) before and after Aniline and MO Removal

samples	BET surface area S_{BET} (m^2/g)	total pore volume (cm^3/g)	average pore diameter (nm)
Fe/MIL-101(Cr)(110 °C-VD)	1683	1.44	2.20
Fe/MIL-101(Cr)(110 °C-VD) recycling (aniline)	745	0.681	2.20
Fe/MIL-101(Cr)(110 °C-VD) recycling (MO)	733	0.681	2.07
Fe/MIL-100(Cr)(110 °C-VD)	555	0.449	2.07
Fe/MIL-100(Cr)(110 °C-VD) recycling (aniline)	495	0.445	2.06
Fe/MIL-100(Cr)(110 °C-VD) recycling (MO)	403	0.449	2.01

4. CONCLUSIONS

This paper focuses on the catalyst preparation, characterization, and the catalytic test of MIL-type MOF-supported Fe catalysts for the advanced oxidation of selected organic compounds in water. Following conclusions are drawn.

(1) The Fe/MIL-100(Cr) and Fe/MIL-101(Cr) catalysts were successfully prepared by using a carrier-gas free VD method, which reinforced that this VD method can be a general tool for preparing MOF-supported Fe catalysts.
(2) With the present preparation process, an Fe loading of 7.8−27.2 wt % can be achieved on Fe/MIL-101(Cr) at a T_d of 110−150 °C. In contrast, Fe/MIL-100(Cr) was prepared using the same method with a Fe loading of only 4.35% at 110 °C. The characterization results showed that most of the Fe components resided uniformly within the pores of the MOF supports.

https://doi.org/10.1021/acsomega.1c03118
ACS Omega 2021, 6, 25311−25322

(3) Both Fe/MIL-100(Cr) and Fe/MIL-101(Cr) were rather effective for the catalytic removal of aniline from water. Fe/MIL-100(Cr) could effectively remove the TOC value of aniline, while Fe/MIL-101(Cr) had a lower TOC removal efficiency. Both catalysts can also efficiently catalyze the removal of MO by H_2O_2 in an aqueous solution, however, both of them had a certain adsorption effect on MO.

(4) The rather good catalytic performances for organic compound degradation were obtained with a neutral instead of acidic solution, which is of great significance for potential applications of the catalysts in the AOP processes.

(5) Both of the Fe/MIL-100(Cr) and Fe/MIL-101(Cr) catalysts showed good stability in the crystalline form compared to the previously prepared Fe/UiO-66 catalyst.[49]

AUTHOR INFORMATION

Corresponding Author

Xufeng Lin − *Department of Chemistry, College of Science and State Key Laboratory of Heavy Oil Processing, China University of Petroleum (East China), Qingdao 266580, P. R. China;* orcid.org/0000-0003-0256-9092; Email: hatrick2009@upc.edu.cn

Authors

Huimin Zhuang − *Department of Chemistry, College of Science, China University of Petroleum (East China), Qingdao 266580, P. R. China*

Wumin Zhang − *Department of Chemistry, College of Science, China University of Petroleum (East China), Qingdao 266580, P. R. China*

Lu Wang − *College of Chemical Engineering, China University of Petroleum (East China), Qingdao 266580, P. R. China*

Yuanyuan Zhu − *College of Chemical Engineering, China University of Petroleum (East China), Qingdao 266580, P. R. China*

Yanyan Xi − *College of Chemical Engineering and State Key Laboratory of Heavy Oil Processing, China University of Petroleum (East China), Qingdao 266580, P. R. China*

Complete contact information is available at: https://pubs.acs.org/10.1021/acsomega.1c03118

Author Contributions

‖H.Z. and W.Z. contributed equally to this work.

Notes

The authors declare no competing financial interest.

ACKNOWLEDGMENTS

Support from the National Natural Science Foundation of China (21576291) and Shandong Province Natural Science Foundation (ZR2014BM002) is gratefully acknowledged.

REFERENCES

(1) Ai, L.; Zhang, C.; Li, L.; Jiang, J. Iron terephthalate metal−organic framework: Revealing the effective activation of hydrogen peroxide for the degradation of organic dye under visible light irradiation. *Appl. Catal., B* **2014**, *148*−*149*, 191−200.

(2) Xu, H.-y.; Prasad, M.; Liu, Y. Schorl: A novel catalyst in mineral-catalyzed Fenton-like system for dyeing wastewater discoloration. *J. Hazard. Mater.* **2009**, *165*, 1186−1192.

(3) Panda, N.; Sahoo, H.; Mohapatra, S. Decolourization of Methyl Orange using Fenton-like mesoporous Fe_2O_3−SiO_2 composite. *J. Hazard. Mater.* **2011**, *185*, 359−365.

(4) El-Monaem, E. M. A.; El-Latif, M. M. A.; Eltaweil, A. S.; El-Subruiti, G. M. Cobalt nanoparticles supported on reduced amine-functionalized graphene oxide for catalytic reduction of nitroanilines and organic dyes. *Nano* **2021**, *16*, 2150039.

(5) Eltaweil, A. S.; El-Tawil, A. M.; Abd El-Monaem, E. M.; El-Subruiti, G. M. Zero Valent Iron Nanoparticle-Loaded Nanobentonite Intercalated Carboxymethyl Chitosan for Efficient Removal of Both Anionic and Cationic Dyes. *ACS Omega* **2021**, *6*, 6348−6360.

(6) Xue, G.; Wang, Q.; Qian, Y.; Gao, P.; Su, Y.; Liu, Z.; Chen, H.; Li, X.; Chen, J. Simultaneous removal of aniline, antimony and chromium by ZVI coupled with H_2O_2: Implication for textile wastewater treatment. *J. Hazard. Mater.* **2019**, *368*, 840−848.

(7) El-Subruiti, G. M.; Eltaweil, A. S.; Sallam, S. A. Synthesis of Active MFe_2O_4/γ-Fe_2O_3 Nanocomposites (Metal = Ni or Co) for Reduction of Nitro-Containing Pollutants and Methyl Orange Degradation. *Nano* **2019**, *14*, 1950125.

(8) Lee, J.-M.; Kim, J.-H.; Chang, Y.-Y.; Chang, Y.-S. Steel dust catalysis for Fenton-like oxidation of polychlorinated dibenzo-p-dioxins. *J. Hazard. Mater.* **2009**, *163*, 222−230.

(9) Wang, J. L.; Xu, L. J. Advanced Oxidation Processes for Wastewater Treatment: Formation of Hydroxyl Radical and Application. *Crit. Rev. Environ. Sci. Technol.* **2012**, *42*, 251−325.

(10) Wang, J.; Bai, Z. Fe-based catalysts for heterogeneous catalytic ozonation of emerging contaminants in water and wastewater. *Chem. Eng. J.* **2017**, *312*, 79−98.

(11) Yang, X.-j.; Xu, X.-m.; Xu, J.; Han, Y.-f. Iron Oxychloride (FeOCl): An Efficient Fenton-Like Catalyst for Producing Hydroxyl Radicals in Degradation of Organic Contaminants. *J. Am. Chem. Soc.* **2013**, *135*, 16058−16061.

(12) Xu, L.; Wang, J. A heterogeneous Fenton-like system with nanoparticulate zero-valent iron for removal of 4-chloro-3-methyl phenol. *J. Hazard. Mater.* **2011**, *186*, 256−264.

(13) Oller, I.; Malato, S.; Sánchez-Pérez, J. A. Combination of Advanced Oxidation Processes and biological treatments for wastewater decontamination—A review. *Sci. Total Environ.* **2011**, *409*, 4141−4166.

(14) Matilainen, A.; Sillanpää, M. Removal of natural organic matter from drinking water by advanced oxidation processes. *Chemosphere* **2010**, *80*, 351−365.

(15) Brillas, E.; Sirés, I.; Oturan, M. A. Electro-Fenton Process and Related Electrochemical Technologies Based on Fenton's Reaction Chemistry. *Chem. Rev.* **2009**, *109*, 6570−6631.

(16) Xu, Z.; Fang, D.; Shi, W.; Xu, J.; Lu, A.; Wang, K.; Zhou, L. Enhancement in Photo-Fenton-Like Degradation of Azo Dye Methyl Orange Using TiO_2/Hydroniumjarosite Composite Catalyst. *Environ. Eng. Sci.* **2015**, *32*, 497−504.

(17) Yu, L.; Chen, J.; Liang, Z.; Xu, W.; Chen, L.; Ye, D. Degradation of phenol using Fe_3O_4-GO nanocomposite as a heterogeneous photo-Fenton catalyst. *Sep. Purif. Technol.* **2016**, *171*, 80−87.

(18) Qian, X.; Ren, M.; Zhu, Y.; Yue, D.; Han, Y.; Jia, J.; Zhao, Y. Visible Light Assisted Heterogeneous Fenton-Like Degradation of Organic Pollutant via α-FeOOH/Mesoporous Carbon Composites. *Environ. Sci. Technol.* **2017**, *51*, 3993−4000.

(19) Georgiou, D.; Hatiras, J.; Aivasidis, A. Microbial immobilization in a two-stage fixed-bed-reactor pilot plant for on-site anaerobic decolorization of textile wastewater. *Enzyme Microb. Technol.* **2005**, *37*, 597−605.

(20) Wang, Q.; Tian, S.; Ning, P. Ferrocene-Catalyzed Heterogeneous Fenton-like Degradation of Methylene Blue: Influence of Initial Solution pH. *Ind. Eng. Chem. Res.* **2014**, *53*, 6334−6340.

(21) Huang, Y.-H.; Su, C.-C.; Yang, Y.-P.; Lu, M.-C. Degradation of aniline catalyzed by heterogeneous Fenton-like reaction using iron oxide/SiO_2. *Environ. Prog. Sustainable Energy* **2013**, *32*, 187−192.

(22) Xiao, F.; Li, W.; Fang, L.; Wang, D. Synthesis of akageneite (beta-FeOOH)/reduced graphene oxide nanocomposites for oxida-

tive decomposition of 2-chlorophenol by Fenton-like reaction. *J. Hazard. Mater.* **2016**, *308*, 11−20.
(23) Wang, Y.; Priambodo, R.; Zhang, H.; Huang, Y.-H. Degradation of the azo dye Orange G in a fluidized bed reactor using iron oxide as a heterogeneous photo-Fenton catalyst. *RSC Adv.* **2015**, *5*, 45276−45283.
(24) Shukla, P.; Wang, S.; Sun, H.; Ang, H.-M.; Tadé, M. Adsorption and heterogeneous advanced oxidation of phenolic contaminants using Fe loaded mesoporous SBA-15 and H_2O_2. *Chem. Eng. J.* **2010**, *164*, 255−260.
(25) Hou, X.; Huang, X.; Ai, Z.; Zhao, J.; Zhang, L. Ascorbic acid/Fe@Fe_2O_3: A highly efficient combined Fenton reagent to remove organic contaminants. *J. Hazard. Mater.* **2016**, *310*, 170−178.
(26) Huo, S.-H.; Yan, X.-P. Facile magnetization of metal−organic framework MIL-101 for magnetic solid-phase extraction of polycyclic aromatic hydrocarbons in environmental water samples. *Analyst* **2012**, *137*, 3445−3451.
(27) Gao, Y.; Li, S.; Li, Y.; Yao, L.; Zhang, H. Accelerated photocatalytic degradation of organic pollutant over metal-organic framework MIL-53(Fe) under visible LED light mediated by persulfate. *Appl. Catal., B* **2017**, *202*, 165−174.
(28) Wang, J.-L.; Wang, C.; Lin, W. Metal−Organic Frameworks for Light Harvesting and Photocatalysis. *ACS Catal.* **2012**, *2*, 2630−2640.
(29) Watanabe, T.; Sholl, D. S. Accelerating Applications of Metal−Organic Frameworks for Gas Adsorption and Separation by Computational Screening of Materials. *Langmuir* **2012**, *28*, 14114−14128.
(30) Murray, L. J.; Dincă, M.; Long, J. R. Hydrogen storage in metal−organic frameworks. *Chem. Soc. Rev.* **2009**, *38*, 1294−1314.
(31) Attia, N. F.; Jung, M.; Park, J.; Jang, H.; Lee, K.; Oh, H. Flexible nanoporous activated carbon cloth for achieving high H_2, CH_4, and CO_2 storage capacities and selective CO_2/CH_4 separation. *Chem. Eng. J.* **2020**, *379*, 122367.
(32) Park, J.; Jung, M.; Jang, H.; Lee, K.; Attia, N. F.; Oh, H. A facile synthesis tool of nanoporous carbon for promising H_2, CO_2, and CH_4 sorption capacity and selective gas separation. *J. Mater. Chem. A* **2018**, *6*, 23087−23100.
(33) Omer, A. M.; Abd El-Monaem, E. M.; Abd El-Latif, M. M.; El-Subruiti, G. M.; Eltaweil, A. S. Facile fabrication of novel magnetic ZIF-67 MOF@aminated chitosan composite beads for the adsorptive removal of Cr(VI) from aqueous solutions. *Carbohydr. Polym.* **2021**, *265*, 118084.
(34) Eltaweil, A. S.; Elshishini, H. M.; Ghatass, Z. F.; Elsubruiti, G. M. Ultra-high adsorption capacity and selective removal of Congo red over aminated graphene oxide modified Mn-doped UiO-66 MOF. *Powder Technol.* **2021**, *379*, 407−416.
(35) Eltaweil, A. S.; Abd El-Monaem, E. M.; Omer, A. M.; Khalifa, R. E.; Abd El-Latif, M. M.; El-Subruiti, G. M. Efficient removal of toxic methylene blue (MB) dye from aqueous solution using a metal-organic framework (MOF) MIL-101(Fe): isotherms, kinetics and thermodynamic studies. *Desalin. Water Treat.* **2020**, *189*, 395−407.
(36) Eltaweil, A. S.; Abd El-Monaem, E. M.; El-Subruiti, G. M.; Abd El-Latif, M. M.; Omer, A. M. Fabrication of UiO-66/MIL-101(Fe) binary MOF/carboxylated-GO composite for adsorptive removal of methylene blue dye from aqueous solutions. *RSC Adv.* **2020**, *10*, 19008−19019.
(37) Wei, X.; Wang, C.-C.; Li, Y.; Wang, P.; Wei, Q. The Z-scheme NH_2-UiO-66/PTCDA composite for enhanced photocatalytic Cr(VI) reduction under low-power LED visible light. *Chemosphere* **2021**, *280*, 130734.
(38) Chen, D.-D.; Yi, X.-H.; Ling, L.; Wang, C.-C.; Wang, P. Photocatalytic Cr(VI) sequestration and photo-Fenton bisphenol A decomposition over white light responsive PANI/MIL-88A(Fe). *Appl. Organomet. Chem.* **2020**, *34*, No. e5795.
(39) Wang, J.-W.; Qiu, F.-G.; Wang, P.; Ge, C.; Wang, C.-C. Boosted bisphenol A and Cr(VI) cleanup over Z-scheme WO_3/MIL-100(Fe) composites under visible light. *J. Cleaner Prod.* **2021**, *279*, 123408.
(40) Du, X.; Yi, X.; Wang, P.; Deng, J.; Wang, C.-c. Enhanced photocatalytic Cr(VI) reduction and diclofenac sodium degradation under simulated sunlight irradiation over MIL-100(Fe)/g-C_3N_4 heterojunctions. *Chin. J. Catal.* **2019**, *40*, 70−79.
(41) Liu, N.; Huang, W.; Zhang, X.; Tang, L.; Wang, L.; Wang, Y.; Wu, M. Ultrathin graphene oxide encapsulated in uniform MIL-88A(Fe) for enhanced visible light-driven photodegradation of RhB. *Appl. Catal., B* **2018**, *221*, 119−128.
(42) Farrusseng, D.; Aguado, S.; Pinel, C. Metal−Organic Frameworks: Opportunities for Catalysis. *Angew. Chem., Int. Ed.* **2009**, *48*, 7502−7513.
(43) Ou, S.; Wu, C.-D. Rational construction of metal−organic frameworks for heterogeneous catalysis. *Inorg. Chem. Front.* **2014**, *1*, 721−734.
(44) Lv, H.; Zhao, H.; Cao, T.; Qian, L.; Wang, Y.; Zhao, G. Efficient degradation of high concentration azo-dye wastewater by heterogeneous Fenton process with iron-based metal-organic framework. *J. Mol. Catal. A: Chem.* **2015**, *400*, 81−89.
(45) Niu, H.; Zheng, Y.; Wang, S.; Zhao, L.; Yang, S.; Cai, Y. Continuous generation of hydroxyl radicals for highly efficient elimination of chlorophenols and phenols catalyzed by heterogeneous Fenton-like catalysts yolk/shell Pd@Fe_3O_4@metal organic frameworks. *J. Hazard. Mater.* **2018**, *346*, 174−183.
(46) Vu, T. A.; Le, G. H.; Dao, C. D.; Dang, L. Q.; Nguyen, K. T.; Dang, P. T.; Tran, H. T. K.; Duong, Q. T.; Nguyen, T. V.; Lee, G. D. Isomorphous substitution of Cr by Fe in MIL-101 framework and its application as a novel heterogeneous photo-Fenton catalyst for reactive dye degradation. *RSC Adv.* **2014**, *4*, 41185−41194.
(47) Férey, G. Hybrid porous solids: past, present, future. *Chem. Soc. Rev.* **2008**, *37*, 191−214.
(48) Xu, L.; Lin, X.; Xi, Y.; Lu, X.; Wang, C.; Liu, C. Alumina-supported Fe catalyst prepared by vapor deposition and its catalytic performance for oxidative dehydrogenation of ethane. *Mater. Res. Bull.* **2014**, *59*, 254−260.
(49) Zhuang, H.; Chen, B.; Cai, W.; Xi, Y.; Ye, T.; Wang, C.; Lin, X. UiO-66-supported Fe catalyst: a vapour deposition preparation method and its superior catalytic performance for removal of organic pollutants in water. *R. Soc. Open Sci.* **2019**, *6*, 182047−182060.
(50) Li, Y.; Liu, H.; Li, W.-J.; Zhao, F.-Y.; Ruan, W.-J. A nanoscale Fe(II) metal−organic framework with a bipyridinedicarboxylate ligand as a high performance heterogeneous Fenton catalyst. *RSC Adv.* **2016**, *6*, 6756−6760.
(51) Férey, G.; Serre, C.; Mellot-Draznieks, C.; Millange, F.; Surblé, S.; Dutour, J.; Margiolaki, I. A Hybrid Solid with Giant Pores Prepared by a Combination of Targeted Chemistry, Simulation, and Powder Diffraction. *Angew. Chem., Int. Ed.* **2004**, *43*, 6296−6301.
(52) Ferey, G.; Mellot-Draznieks, C.; Serre, C.; Millange, F.; Dutour, J.; Surble, S.; Margiolaki, I. A Chromium Terephthalate-Based Solid with Unusually Large Pore Volumes and Surface Area. *Science* **2005**, *309*, 2040−2042.
(53) Wang, C.; Zheng, M.; Lin, W. Asymmetric Catalysis with Chiral Porous Metal−Organic Frameworks: Critical Issues. *J. Phys. Chem. Lett.* **2011**, *2*, 1701−1709.
(54) Kim, M. J.; Park, S. M.; Song, S.-J.; Won, J.; Lee, J. Y.; Yoon, M.; Kim, K.; Seo, G. Adsorption of pyridine onto the metal organic framework MIL-101. *J. Colloid Interface Sci.* **2011**, *361*, 612−617.
(55) Liu, B.; Chai, Y.; Wang, Y.; Zhang, T.; Liu, Y.; Liu, C. A simple technique for preparation of presulfided eggshell MoS_2/Al_2O_3 catalysts and kinetics approach for highly selective hydrodesulfurization of FCC gasoline. *Appl. Catal., A* **2010**, *388*, 248−255.
(56) Peng, L.; Zhang, J.; Li, J.; Han, B.; Xue, Z.; Yang, G. Surfactant-directed assembly of mesoporous metal−organic framework nanoplates in ionic liquids. *Chem. Commun.* **2012**, *48*, 8688−8690.
(57) Horcajada, P.; Surblé, S.; Serre, C.; Hong, D.-Y.; Seo, Y.-K.; Chang, J.-S.; Grenèche, J.-M.; Margiolaki, I.; Férey, G. Synthesis and catalytic properties of MIL-100(Fe), an iron(iii) carboxylate with large pores. *Chem. Commun.* **2007**, 2820−2822.
(58) Ling, F.; Fang, L.; Lu, Y.; Gao, J.; Wu, F.; Zhou, M.; Hu, B. A novel CoFe layered double hydroxides adsorbent: High adsorption

amount for methyl orange dye and fast removal of Cr(IV). *Microporous Mesoporous Mater.* **2016**, *234*, 230−238.
(59) Tang, H.; Li, J.; Bie, Y.; Zhu, L.; Zou, J. Photochemical removal of aniline in aqueous solutions: Switching from photocatalytic degradation to photo-enhanced polymerization recovery. *J. Hazard. Mater.* **2010**, *175*, 977−984.
(60) Zhu, L.; Lv, M.; Dai, X.; Xu, X.; Qi, H.; Yu, Y. Reaction kinetics of the degradation of chloroanilines and aniline by aerobic granule. *Biochem. Eng. J.* **2012**, *68*, 215−220.
(61) Hu, R.; Wang, X.; Dai, S.; Shao, D.; Hayat, T.; Alsaedi, A. Application of graphitic carbon nitride for the removal of Pb(II) and aniline from aqueous solutions. *Chem. Eng. J.* **2015**, *260*, 469−477.
(62) Matsushita, M.; Kuramitz, H.; Tanaka, S. Electrochemical Oxidation for Low Concentration of Aniline in Neutral pH Medium: Application to the Removal of Aniline Based on the Electrochemical Polymerization on a Carbon Fiber. *Environ. Sci. Technol.* **2005**, *39*, 3805−3810.
(63) Sheng-tao, J.; Jian-zhong, Z.; Shu-li, B.; Yu-jiang, G.; Jun, Y. Research on Fe-loaded ZSM-5 molecular sieve catalyst in high concentration aniline wastewater treatment. *Desalin. Water Treat.* **2016**, *57*, 791−798.
(64) Tang, J.; Wang, J. Fe-based metal organic framework/graphene oxide composite as an efficient catalyst for Fenton-like degradation of methyl orange. *RSC Adv.* **2017**, *7*, 50829−50837.
(65) Tong, M.; Liu, D.; Yang, Q.; Devautour-Vinot, S.; Maurin, G.; Zhong, C. Influence of framework metal ions on the dye capture behavior of MIL-100 (Fe, Cr) MOF type solids. *J. Mater. Chem. A* **2013**, *1*, 8534−8537.
(66) Joseph, J. M.; Destaillats, H.; Hung, H.-M.; Hoffmann, M. R. The Sonochemical Degradation of Azobenzene and Related Azo Dyes: Rate Enhancements via Fenton's Reactions. *J. Phys. Chem. A* **2000**, *104*, 301−307.

https://doi.org/10.1021/acsomega.1c03118
ACS Omega 2021, 6, 25311−25322